Chapter 8
Real-Time Noise Cancellation Using Wavelet Transforms

Ehsan Sheybani

Introduction

Noise from different sources can have dramatic effects on the performance and decision-making process of the systems. As such, total elimination of the noise could also be damaging to the final outcome, as it may result in removing useful information that can benefit the decision-making process. Several efforts have been made to find the optimal balance between noise and data parameters. For the most part, experts in the field agree that it is more beneficial to remove noise at the node level where data is collected [1–3]. This is mainly stressed so that the low-power, low bandwidth, and low computational overhead constraints are met while fused datasets can still be used to make reliable decisions [4–6].

Digital signal processing algorithms, based on advanced mathematical concepts, have long served to manipulate data to be a good fit for analysis and synthesis of any kind. For the noise removal application, a special wavelet-based approach has been considered to suppress the effect of noise in data. The proposed technique uses the orthogonality properties of wavelets to decompose the dataset into spaces of coarse and detailed signals. With the filter banks being designed from special bases for this specific application, the output signal in this case would be components of the original signal represented at different time and frequency scales and translations. A detailed description of the techniques follows in the next section.

Ehsan Sheybani (✉)
Virginia State University, Petersburg, VA, USA
e-mail: esheybani@vsu.edu

B. Toni (ed.), *Advances in Interdisciplinary Mathematical Research*, Springer Proceedings in Mathematics & Statistics 37, DOI 10.1007/978-1-4614-6345-0_8,

Wavelet-Based Transforms

Traditionally, Fourier transform (FT) has been applied to time-domain signals for signal processing tasks such as noise removal. The shortcoming of the FT is in its dependence on time averaging over entire duration of the signal. Due to its short time span, analysis of dataset requires resolution in particular time and frequency rather than frequency alone. Wavelets are the result of translation and scaling of a finite-length waveform known as mother wavelet. A wavelet divides a function into its frequency components such that its resolution matches the frequency scale and translation. To represent a signal in this fashion, it would have to go through a wavelet transform. Application of the wavelet transform to a function results in a set of orthogonal basis functions which are the time-frequency components of the signal. Due to its resolution in both time and frequency, wavelet transform is the best tool for detection and classification of signals that are nonstationary or have discontinuities and sharp peaks. Depending on whether a given function is analyzed in all scales and translations or a subset of them, the continuous (CWT), discrete (DWT), or multi-resolution wavelet transform (MWT) can be applied.

An example of the generating function (mother wavelet) based on the sinc function for the CWT is

$$\psi(t) = 2Sinc(2t) - Sinc(t) = \frac{Sin(2\pi t) - Sin(\pi t)}{\pi t} \tag{1}$$

normalized with scale one frequency band [1, 2]. The subspaces of this function are generated by translation and scaling. For instance, the subspace of scale (dilation) a and translation (shift) b of the above function is

$$\psi_{a,b}(t) = \frac{1}{\sqrt{a}}\psi\left(\frac{t-b}{a}\right) \tag{2}$$

$a > 0$ defines the scale and frequency band [1/a, 2/a], whereas b ϵ R is any real number defining the shift. When a function x is projected into this subspace, an integral would have to be evaluated to calculate the wavelet coefficients in that scale:

$$WT_{\psi}\{x\}(a,b) = \langle x, \psi_{a,b}\rangle = \int_R x(t)\overline{\psi_{a,b}(t)}dt \tag{3}$$

where $\overline{\psi_{a,b}(t)}$ indicates the conjugate of function $\psi_{a,b}$ and $\langle x, \psi_{a,b}\rangle$ is the inner product of $L_2(R)$, the space of square-integrable function over R. And therefore, the function x can be shown in term of its components:

$$x_a(t) = \int_R WT_{\psi}\{x\}(a,b).\psi_{a,b}(t)db \tag{4}$$

projection of x onto the subspace of scale a. Due to computational and time constraints, it is impossible to analyze a function using all wavelet coefficients. Therefore, usually a subset of the discrete coefficients is used to reconstruct the best approximation of the signal. This subset is generated from the discrete version of the generating function with the corresponding wavelet coefficients:

$$\psi_{m,n}(t) = a^{-m/2}\psi\left(a^{-m}t - nb\right). \tag{5}$$

with integers m, n ε Z. Applying this subset to a function x representing a signal with finite energy will result in DWT coefficients from which one can closely approximate (reconstruct) x using the coarse coefficients of this sequence:

$$x(t) = \sum_{m\in Z}\sum_{n\in Z}\langle x, \psi_{m,n}\rangle.\psi_{m,n}(t). \tag{6}$$

The MWT is obtained by choosing a finite number of wavelet coefficients from a set of DWT coefficients. However, to avoid computational complexity, two generating functions ϕ and ψ are used to create the subspaces restricting a to a = 2 and b to b = 1. As a result, we have the subspace $V_m = \text{span}(\phi_{m,n}, n \in Z)$ generated by the coefficients

$$\phi_{m,n}(t) = 2^{-m/2}\phi\left(2^{-m}t - n\right) \tag{7}$$

and the subspace $W_m = \text{span}(\psi_{m,n}, n \in Z)$ generated by the coefficients

$$\psi_{m,n}(t) = 2^{-m/2}\psi\left(2^{-m}t - n\right). \tag{8}$$

The subspace V_m forms a decreasing sequence in $L^2(R)$, with W_m its orthogonal complement from which the two (fast) wavelet transform pairs (MWT) can be generated:

$$\phi(t) = \sqrt{2}\sum_{n\in Z} h_n\phi(2t - n) \tag{9}$$

and

$$\psi(t) = \sqrt{2}\sum_{n\in Z} g_n\phi(2t - n) \tag{10}$$

with $h_n =< \phi_{0,0}, \phi_{-1,n} >$, and $g_n =< \psi_{0,0}, \psi_{-1,n} >$.

In this paper the DWT has been used to suppress noise in a dataset. Due to its ability to extract information in both time and frequency domain, DWT is considered a very powerful tool. The approach consists of decomposing the signal of interest into its detailed and smoothed components (high- and low-frequency). The detailed components of the signal at different levels of resolution localize the time and frequency of the event. Therefore, the DWT can extract the coarse features of the signal (compression) and filter out details at high frequency (noise). DWT has been successfully applied to system analysis for removal of noise [7, 8]. In this paper we present how

DWT can be applied to detect and filter out noise. A detailed discussion of theory and design methodology for the special-purpose filters for this application follows.

Theory of DWT-Based Filters for Noise Suppression

DWT-based filters can be used to localize abrupt changes in signals in time and frequency. Creative techniques have been implemented to suppress noise in datasets using this approach [7–12]. These techniques range in their approach from calculating the wavelet transforms for all circular shifts and selecting the "best" one that minimizes a cost function [9] to using the entropy criterion [10] and adaptively decomposing a signal in a tree structure so as to minimize the entropy of the representation. In this paper a new approach to cancellation of noise in data has been proposed. The discrete Meyer adaptive wavelet (DMAW) is both translation- and scale-invariant and can represent a signal in a multi-scale format. While DMAW is not the best fit for entropy criterion, it is well suited for the proposed noise cancellation purposes [12].

The process to implement DMAW filters starts with discretizing the Meyer wavelets defined by wavelet and scaling functions as

$$\phi(t) = \sqrt{2} \sum_{n \in Z} h_n \phi(2t - n) \tag{11}$$

and

$$\psi(t) = \sqrt{2} \sum_{n \in Z} g_n \phi(2t - n). \tag{12}$$

The masks for these functions are obtained as

$$\left\{ \phi(0), \phi\left(\frac{1}{2^m}\right), \cdots, \phi\left(\frac{M-1}{2^m}\right) \right\} \tag{13}$$

and

$$\left\{ 0, 0, \ldots, 0, \psi(0), \psi\left(\frac{1}{\sigma}\right), \cdots, \psi\left(\frac{N}{\sigma}\right) \right\} \tag{14}$$

As these two masks are convolved, the generating function (mother wavelet) mask (F) can be obtained as

$$F\left(\frac{k}{2^m}\right) (-M \le k \le N) \tag{15}$$

where for every integer k, integers $n_1^k, n_2^k, \ldots.., n_q^k$ can be found to satisfy the inequality

$$-3 < \mu - n_i^k + \frac{k\sigma}{2^m} < \frac{3\sigma}{2^m} (1 \le i \le q). \tag{16}$$

The corresponding values from mother wavelet mask can then be taken to calculate

$$\alpha_i^k = \frac{2^{m/2}}{\sigma} F\left(\frac{\rho_i^k}{2^m}\right),$$

where $\rho_i^k = \left[(\mu - n_i^k)2^m + k\sigma\right]$ $(1 \le i \le q)$ and

$$\frac{c_{-m,k}}{\sqrt{\alpha}} - \sum_{i=1}^{q} c_{ni}\alpha_i^k. \tag{17}$$

Decomposing the re-normalized signal $\frac{c_{-m,k}}{\sqrt{\alpha}}(k \in Z)$ according to the conventional DWT will result in the entire DMAW filter basis for different scales:

$$\frac{c_{-m+1,k}}{\sqrt{\alpha}}, \frac{d_{-m+1,k}}{\sqrt{\alpha}}, \frac{c_{-m+2,k}}{\sqrt{\alpha}}, \frac{d_{-m+2,k}}{\sqrt{\alpha}}, \cdots, \frac{c_{0,k}}{\sqrt{\alpha}}, \frac{d_{0,k}}{\sqrt{\alpha}}. \tag{18}$$

Experimental Results

Noisy Sinusoidal Signal

Figures 8.1, 8.2, and 8.3 show the experimental results for the application of the proposed filter banks to a noisy sinusoidal signal. As is evident from these figures, a signal can be decomposed in as many levels as desired by the application and allowed by the computational constraints. Levels shown from top to bottom represent the coarse to detailed components of the original signal. Once the signal is decomposed to its components, it is easy to do away with pieces that are not needed. For instance, noise, which is the lowermost signal in Fig. 8.1, can be totally discarded. The reconstructed signal is a fairly good approximation of the original signal. Figure 8.2 shows the thresholds and coefficients of the signal being filtered. Figure 8.3 shows the histogram (frequency of components distribution) of the signal.

Comparison to Other Noisy Signals

For comparison purposes, the same filter banks have also been applied to a quad-chirp signal with noise, and the results are shown in Figs. 8.4–8.9. The versions of the signal have been computed and plotted. In each case the coefficients that have remained intact have also been displayed. Finally, in Figs. 8.7–8.16, the histogram for the denoised quad-chirp, auto-regressive, and white noise has been compared to the original signal. The effectiveness of the proposed filter banks and their capability to maintain the important components of the original signal is evident in these figures.

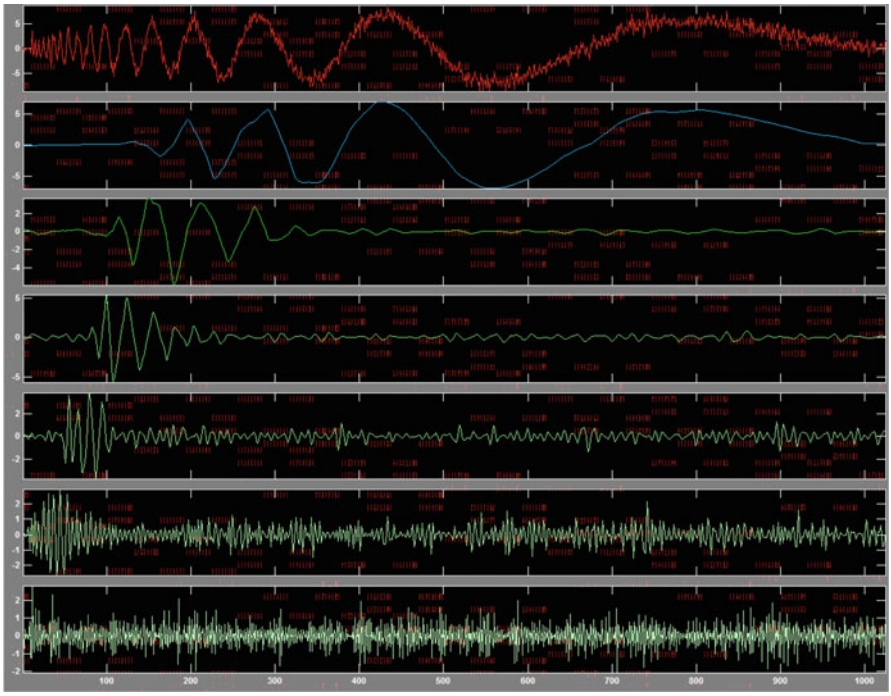

Fig. 8.1 Decomposed signal showing all the components of a mixed sine wave with noise

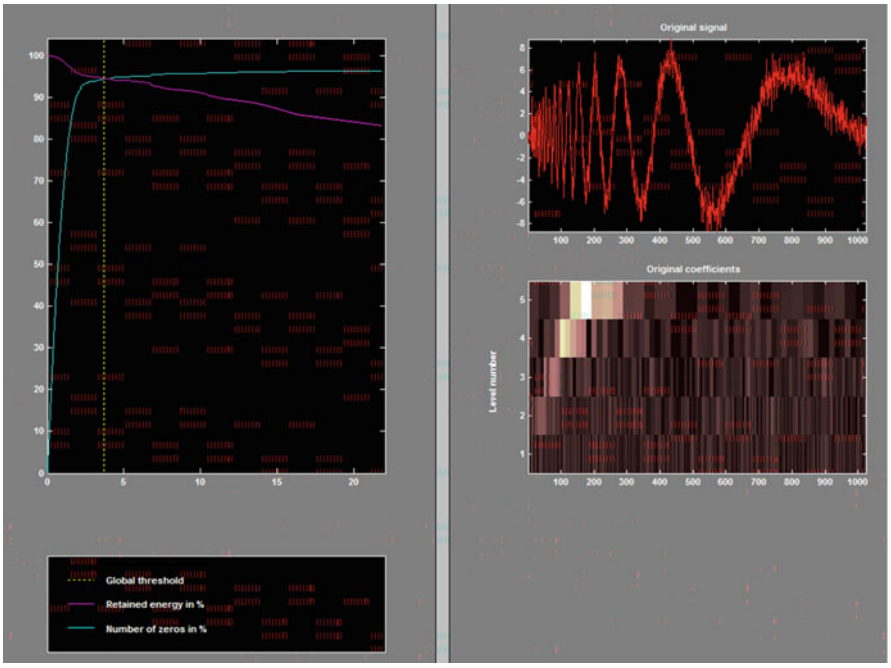

Fig. 8.2 Threshold and coefficients of the decomposed signal

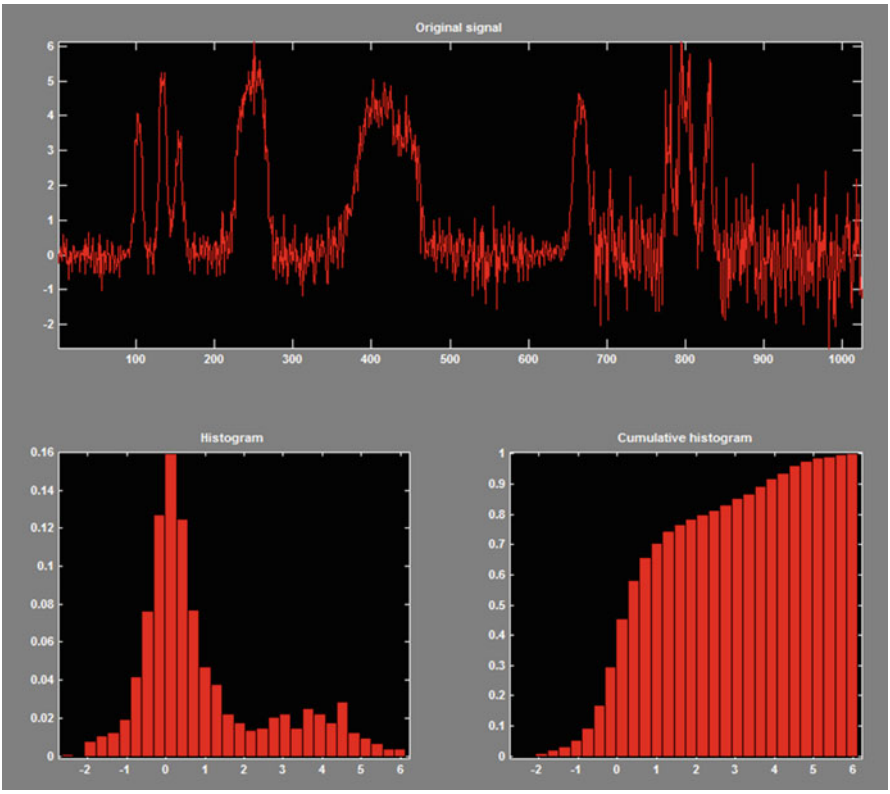

Fig. 8.3 Histogram and cumulative histogram of the signal

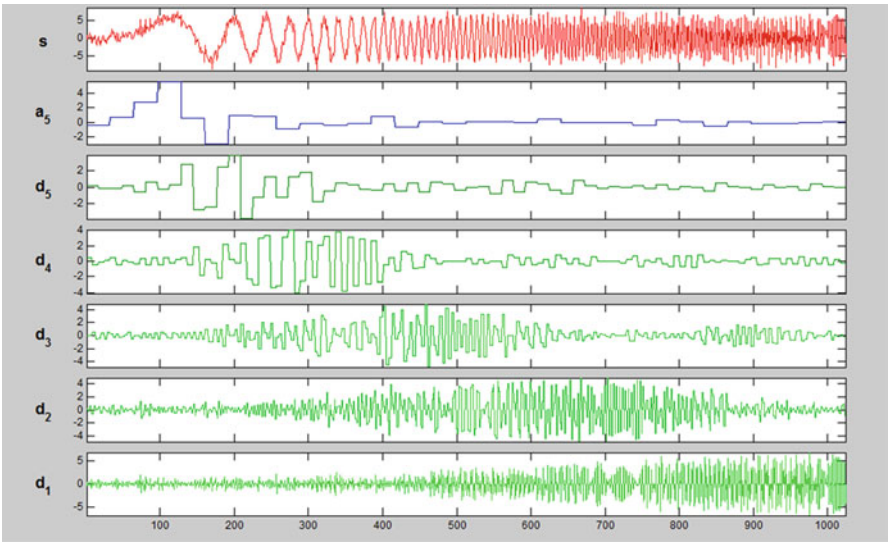

Fig. 8.4 Decomposed signal showing all the components of a quad-chirp wave with noise

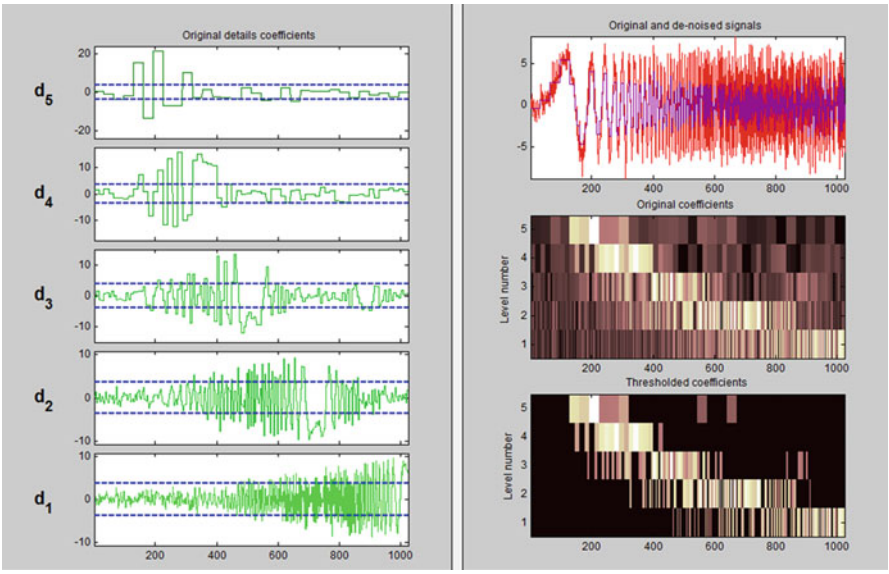

Fig. 8.5 Original and denoised signal with original and thresholded coefficients

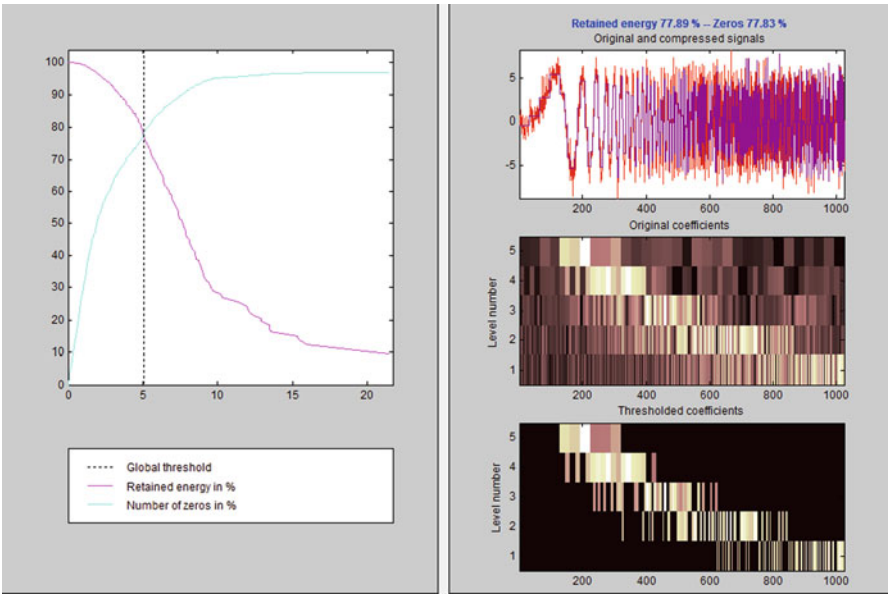

Fig. 8.6 Threshold and coefficients of the decomposed signal showing retained energy and number of zeros

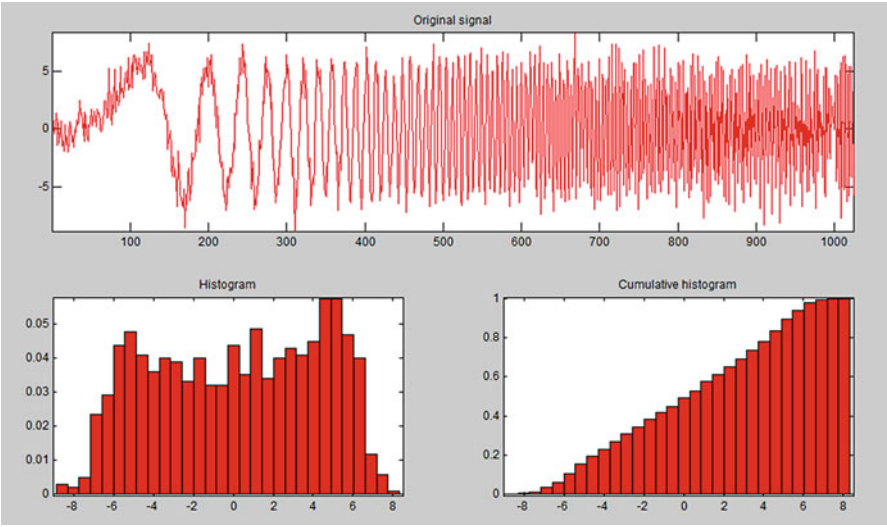

Fig. 8.7 Histogram and cumulative histogram of the original quad-chirp signal

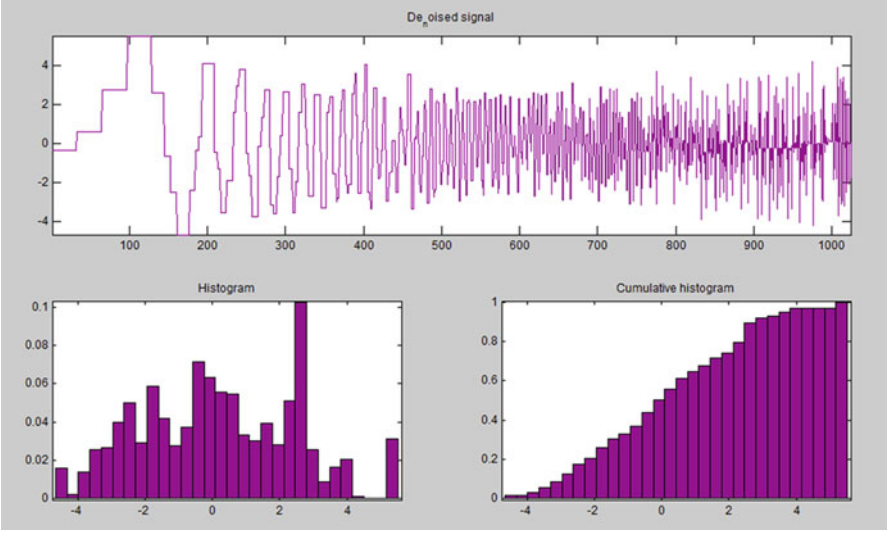

Fig. 8.8 Histogram and cumulative histogram of the denoised quad-chirp signal

Conclusions and Future Work

As expected from the theory, the DMAW filters performed well under noisy conditions. The decomposed signal could be easily freed up from noise. Future plans include the application of these filters to fused datasets and comparison between the

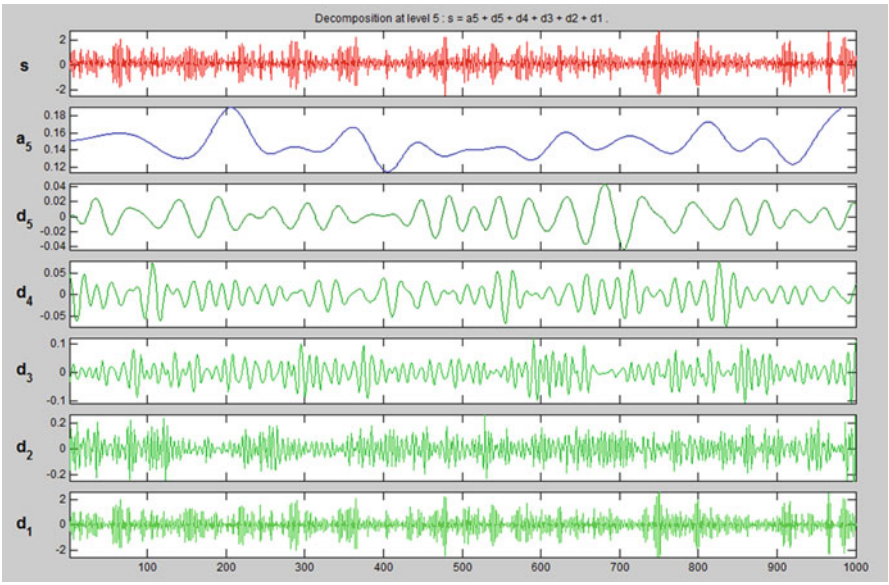

Fig. 8.9 Decomposed signal showing all the components of an auto-regressive wave with noise

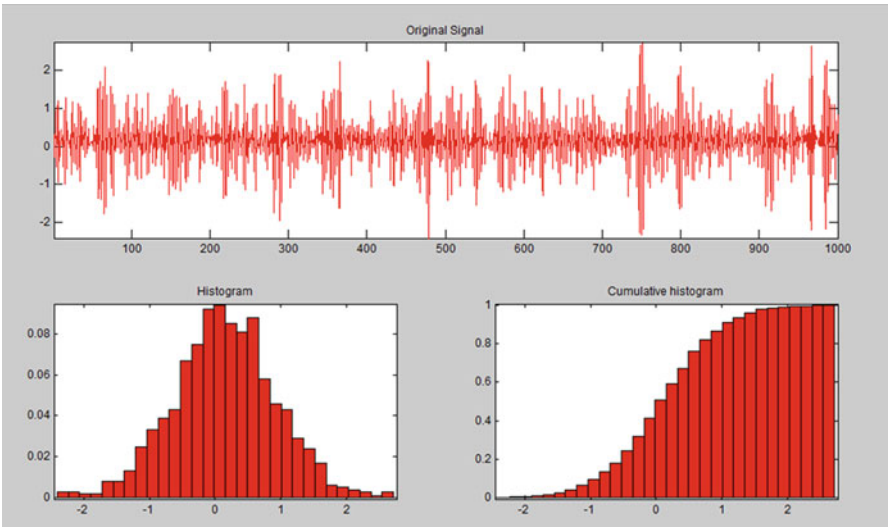

Fig. 8.10 Histogram and cumulative histogram of the original auto-regressive signal

two approaches. Additionally, the results of this study can be used in the decision-making stage to realize the difference this approach can make in accuracy of this process.

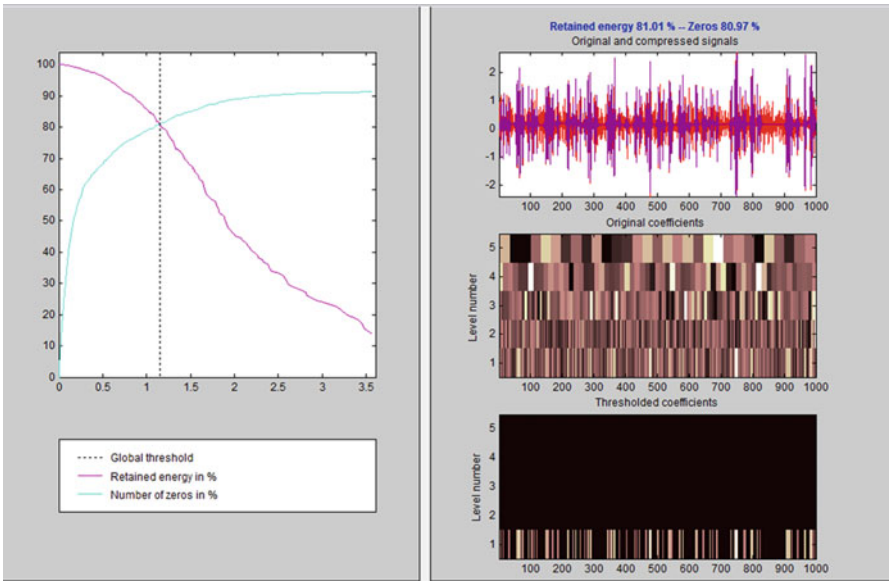

Fig. 8.11 Threshold and coefficients of the decomposed signal showing retained energy and number of zeros

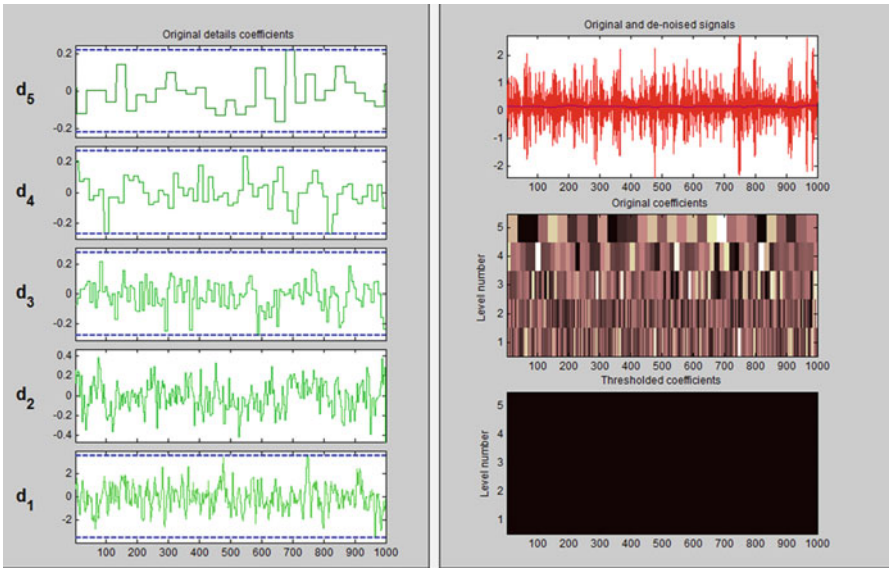

Fig. 8.12 Original and denoised signal with original and thresholded coefficients

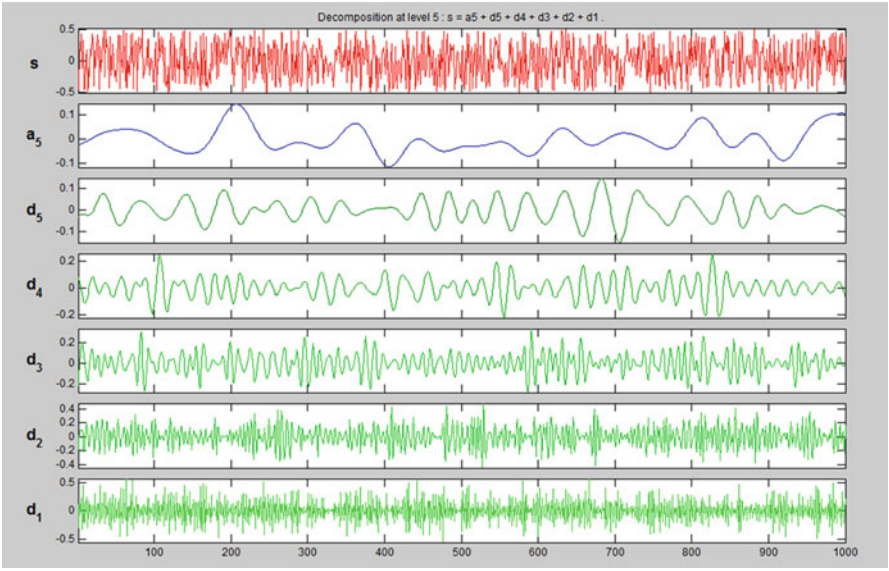

Fig. 8.13 Decomposed signal showing all the components of white noise

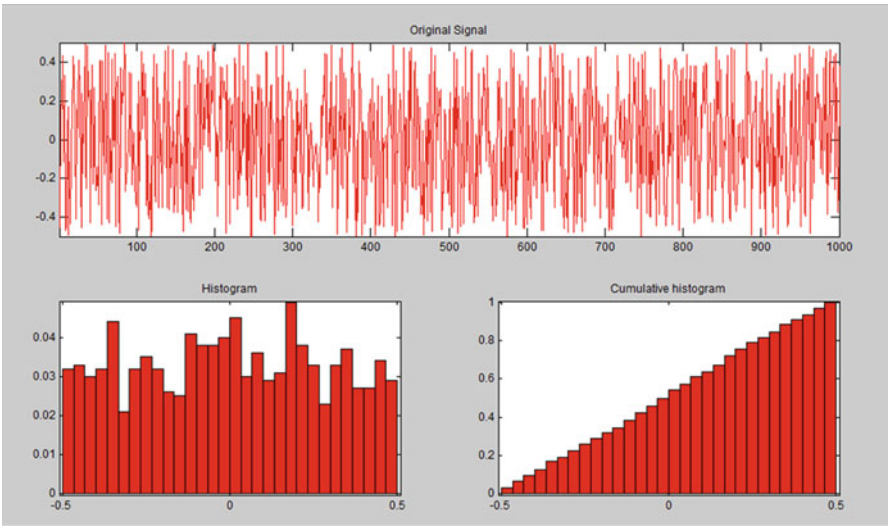

Fig. 8.14 Histogram and cumulative histogram of the original white noise signal

Future work will address issues such as characterizing the parameters for simulation and modeling of the proposed filter for wireless sensor networks, showing how complex examples with correlated sensor data will be filtered for redundancy,

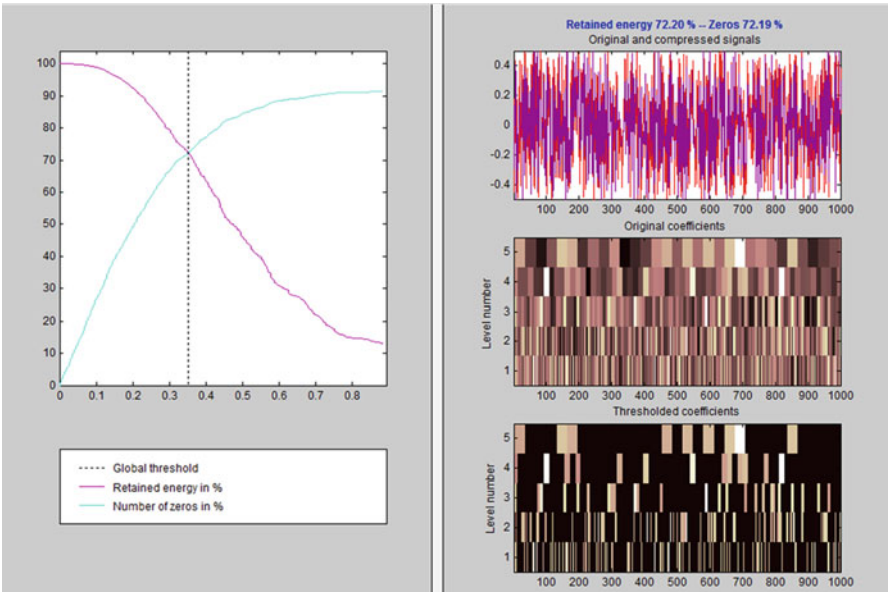

Fig. 8.15 Threshold and coefficients of the decomposed signal showing retained energy and number of zeros

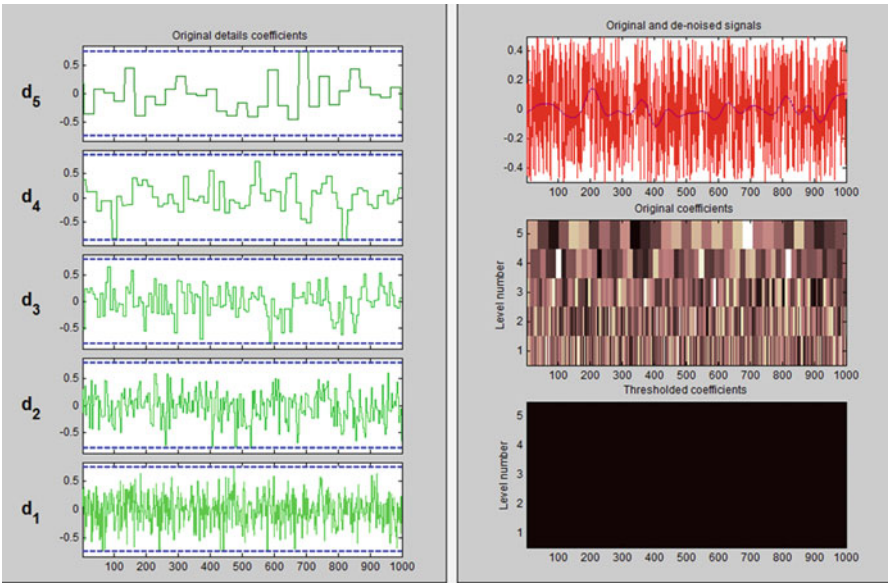

Fig. 8.16 Original and denoised signal with original and thresholded coefficients

and comparing the proposed approach with other similar approaches and giving comparative results to support the claimed advantages, both theoretically and experimentally.

Acknowledgements This is to thank all of the anonymous reviewers and referees who with their constructive comments made this a better chapter for publication.

References

1. Closas, P., Calvo, E., Fernandez-Rubio, J.A., Pages-Zamora, A.: Coupling noise effect in self-synchronizing wireless sensor networks. In: IEEE 8th Workshop on Signal Processing Advances in Wireless Communications, 2007, SPAWC 2007, 17–20 June 2007, pp. 1–5
2. Yamamoto, H., Ohtsuki, T.: Wireless sensor networks with local fusion. In: IEEE Global Telecommunications Conference, 2005, vol. 1, GLOBECOM '05, 28 Nov.–2 Dec. 2005, p. 5
3. Son, S.-H., Kulkarni, S.R., Schwartz, S.C., Roan, M.: Communication-estimation tradeoffs in wireless sensor networks. In: IEEE International Conference on Acoustics, Speech, and Signal Processing, Proceedings, 2005, (ICASSP apos;05), vol. 5, 18–23 March 2005, pp. 1065–1068
4. Abdallah, A., Wolf, W.: Analysis of distributed noise canceling. In: The 2nd International Conference on Distributed Frameworks for Multimedia Applications, 2006, May 2006, pp. 1–7
5. Schizas, I.D., Giannakis, G.B.: Zhi-Quan Luo optimal dimensionality reduction for multisensor fusion in the presence of fading and noise. In: IEEE International Conference on Acoustics, Speech and Signal Processing, 2006. ICASSP 2006 Proceedings. 2006, 14–19 May 2006, vol. 4, pp. IV–IV
6. Pescosolido, L., Barbarossa, S., Scutari, G.: Average consensus algorithms robust against channel noise. In: IEEE 9th Workshop on Signal Processing Advances in Wireless Communications, 2008. SPAWC 2008, 6–9 July 2008, pp. 261–265
7. Cohen, I., Raz, S., Malah, D.: Shift invariant wavelet packet bases. In:Proceedings 20th IEEE Int. Conf. Acoustics, Speech, Signal Processing, Detroit, MI, May 8–12, 1995, pp. 1081–1084
8. Daubechies, I.: Ten lecture on wavelet. In: CBMS-NSF Regional Conference Series in Applied Mathematics. SIAM, Philadelphia, PA (1992)
9. Liang, J., Parks, T.W.: A translation invariant wavelet representation algorithm with applications. IEEE Trans. Signal Process. **44**, 225–232 (1996)
10. Coifman, R.R., Wickhauser, M.V.: Entropy-based algorithms for best basis selection. IEEE Trans. Inform. Theory **38**, 713–718 (1992)
11. Mallat, S.: Zero-crossings of a wavelet transform. IEEE Trans. Inform.Theory **37**, 1019–1033 (1991)
12. Mallat, S., Zhang, S.: Characterization of signals from multiscale edges. IEEE Trans. Pattern Anal. Mach. Intell. **14**, 710–732 (1992)